**Supporting Information**

Continuous g-C$_3$N$_4$ layer coated porous TiO$_2$ fibers with enhanced photocatalytic activity toward H$_2$ evolution and dye degradation

Jing Liu,[a] Jinxiao Zheng,[b] Guichu Yue,[a] Huaike Li,[a] Zhaoyue Liu,[a] Yong Zhao,[a] Nü Wang*[a], Chenghua Sun*[b] and Zhimin Cui*[a]

a. Key Laboratory of Bioinspired Smart Interfacial Science and Technology of Ministry of Education, Beijing Key Laboratory of Bioinspired Energy Materials and Devices, School of Chemistry, Beijing Advanced Innovation Center for Biomedical Engineering, Beihang University, Beijing, 100191 (P. R. China). E-mail: wangn@buaa.edu.cn; cuizhm@buaa.edu.cn

b. Key Laboratory of Photochemical Conversion and Optoelectronic Materials, Technical Institute of Physics and Chemistry, Chinese Academy of Sciences, Beijing 100029 (P. R. China).

c. Inner Mongolia Key Laboratory of Industrial Catalysis, Chemical Engineering College. Inner Mongolia University of Technology, Hohhot, 010051 (P. R. China).
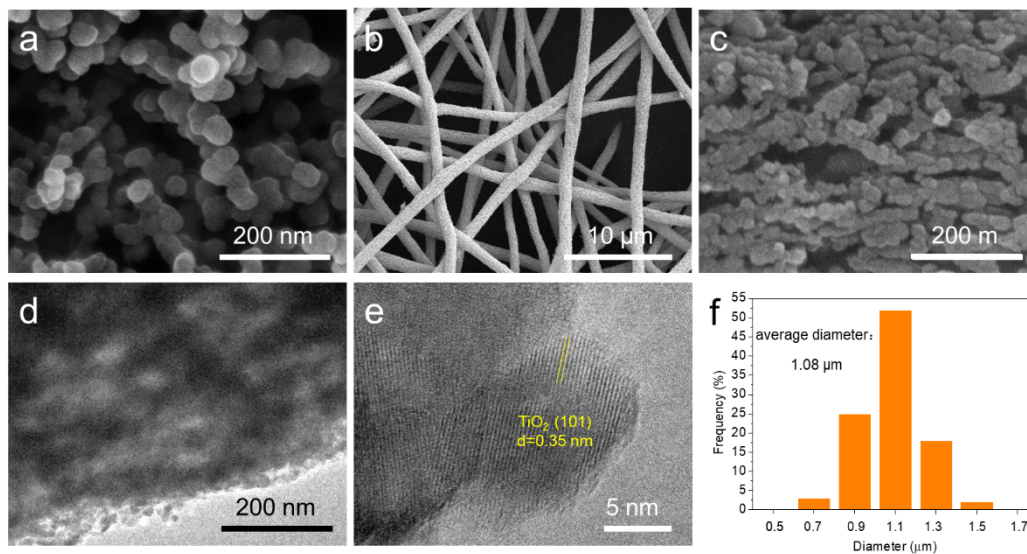
Fig. S1 a) SEM image of CNPs. b) SEM image and magnified image of P-TiO$_2$ fibers. d, e) TEM and HRTEM images of P-TiO$_2$ fibers. f) Diameter distribution of P-TiO$_2$ fibers. The average diameter is 1.08 μm.
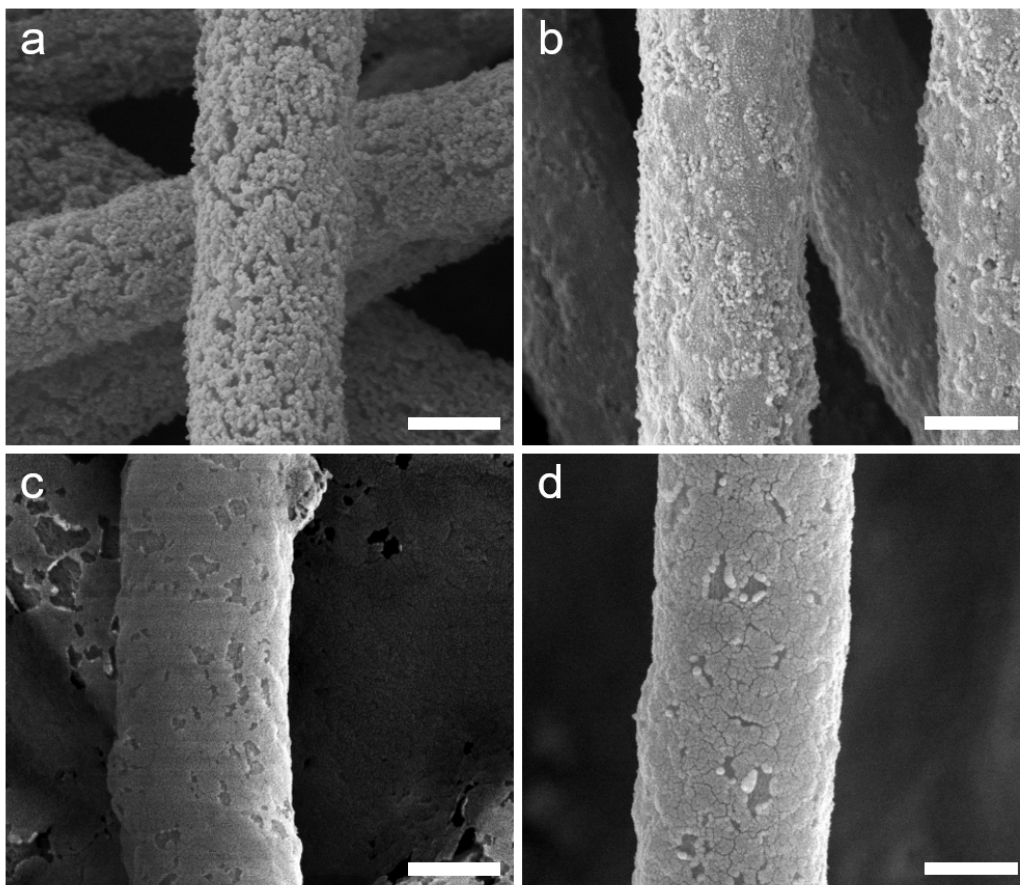
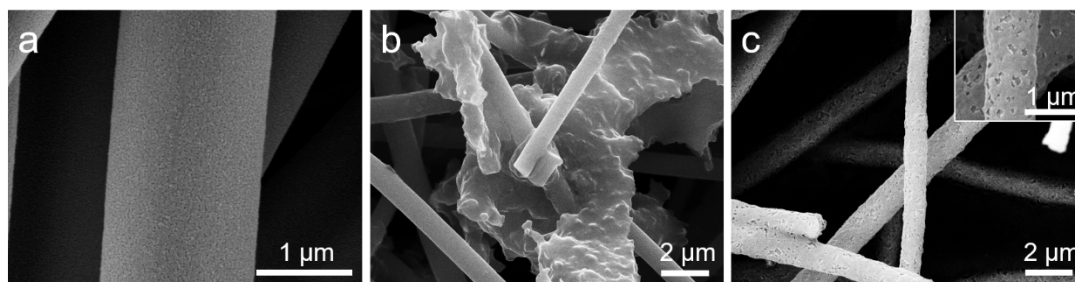**Fig. S2** SEM images of a) P-TiO$_2$ fibers, b-d) PTCN-30%, PTCN-70% and PTCN-90% fibers. Scale bars are 1 μm.

CY solution with different concentration was used to prepare PTCN composite fibers to explore the effect of g-C$_3$N$_4$ content in the heterojunction. The synthesized HPCN fibers are labelled as HPCN-x (x = 30%, 70%, 90%), x is the volume concentration of CY solution. At the same time, P-TiO$_2$ fibers and g-C$_3$N$_4$ were fabricated by the traditional calcination as the previously mentioned method. Surface SEM image of P-TiO$_2$ fibers and PTCN fibers are shown in Fig. S3. When the concentration of CY is 30%, the porous structure keeps well in the PTCN fibers. When the concentration of CY is 70%, g-C$_3$N$_4$ almost form a full coverage on the surface of P-TiO$_2$. The thin g-C$_3$N$_4$ layer wraps around the P-TiO$_2$ fiber and exhibit a core-shell structure. The thickness of the shell increases with increasing the CY concentration to 90%. However, cracks emerged in g-C$_3$N$_4$

layer due to the agglomeration of g-C$_3$N$_4$. Porous structure disappeared on the surface when the CY

concentration is more than 70%. It is ascribed to plenty of g-C$_3$N$_4$ wrap around TiO$_2$ grains forming

a core-shell structure and blocking the pores.
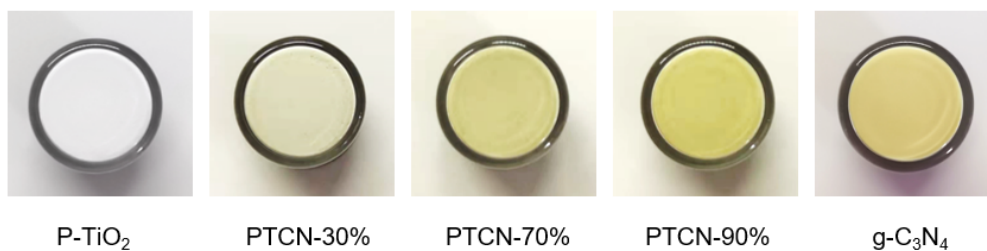
**Fig. S3** Optical images of P-TiO$_2$, PTCN-30%, PTCN-70%, PTCN-90% and pristine g-C$_3$N$_4$.

G-C$_3$N$_4$ exhibits conventional faint yellow and P-TiO$_2$ fibers presents pure white. PTCN

composite fibers show different shades of yellow. The color ranges from light to dark correspond

to the amount of g-C$_3$N$_4$ is changed from small quantity to large quantity in PTCN composite.

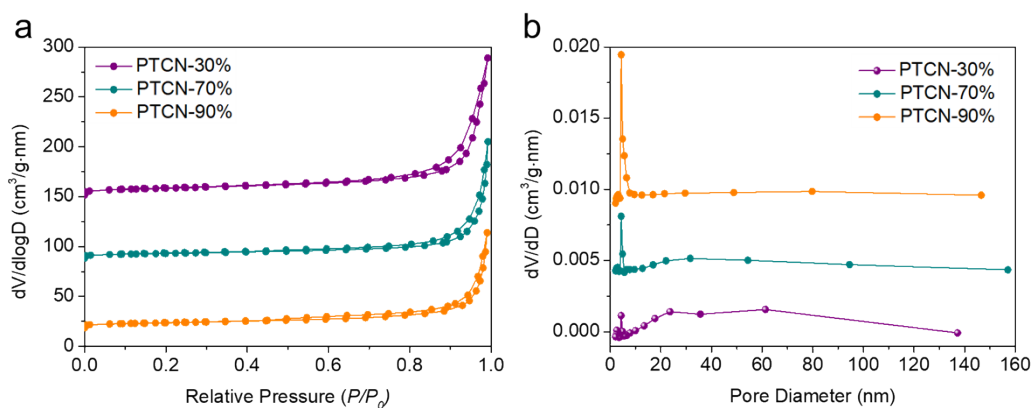**Fig. S4** SEM images of a) S-TiO$_2$ fibers, b) S-TiO$_2$/C$_3$N$_4$-90% fibers, c) PTCN-90% fibers. Inset shows amplified image of PTCN-90% fibers.
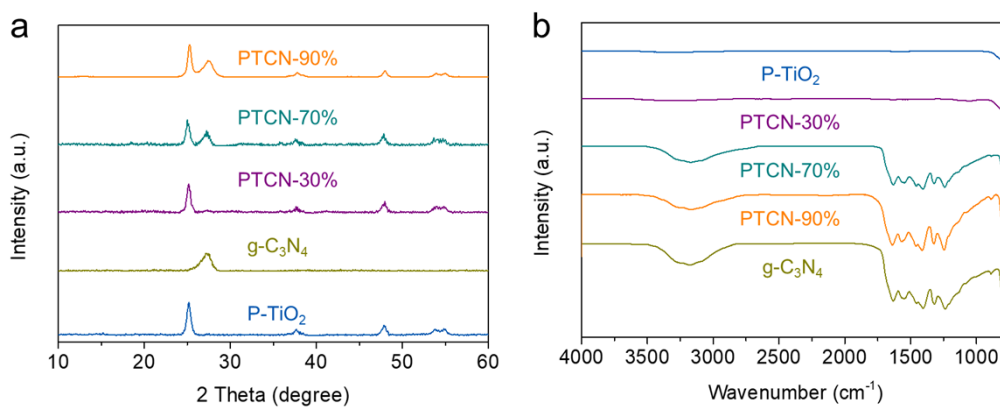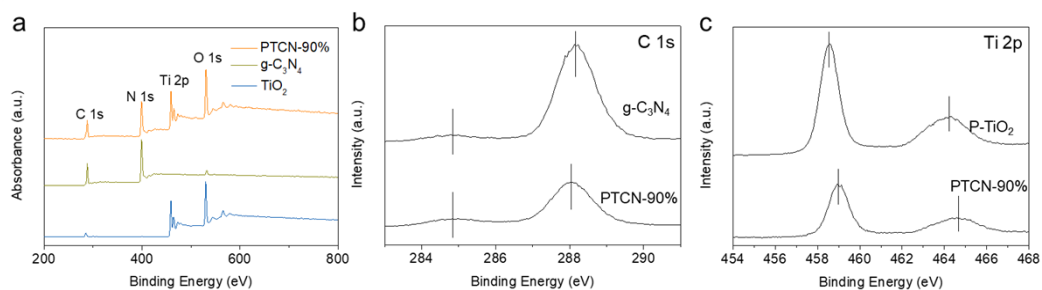

Fig. S5 XRD patterns and FTIR images of P-TiO$_2$, g-C$_3$N$_4$, PTCN-30%, PTCN-70% and PTCN-90%.
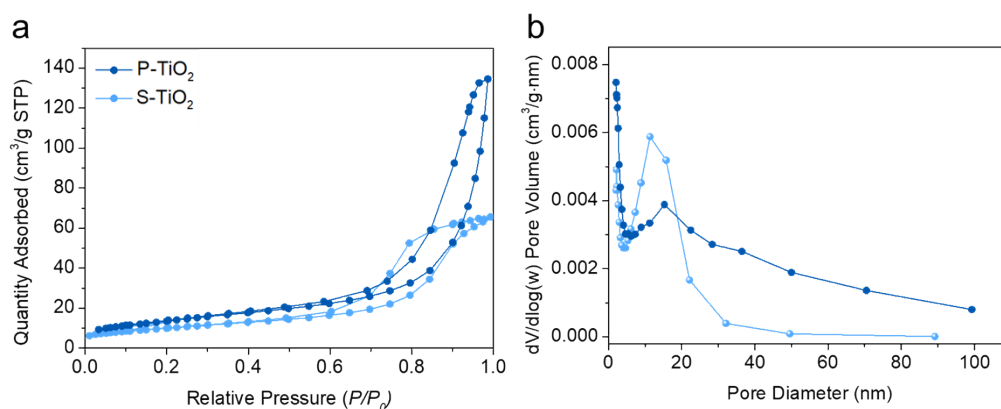
Fig. S6 N$_2$ adsorption-desorption isotherms and corresponding pore size distributions of P-TiO$_2$, and S-TiO$_2$.

Fig. S7 N$_2$ adsorption-desorption isotherms and corresponding pore size distributions of PTCN-30%, PTCN-70% and PTCN-90%.

Fig. S8 a) XPS survey spectra of PTCN, indicating the existence of C, N, Ti and O elements. b, c) High resolution XPS spectra of C 1s and Ti 2p of PTCN-90%, g-C$_3$N$_4$ and P-TiO$_2$.
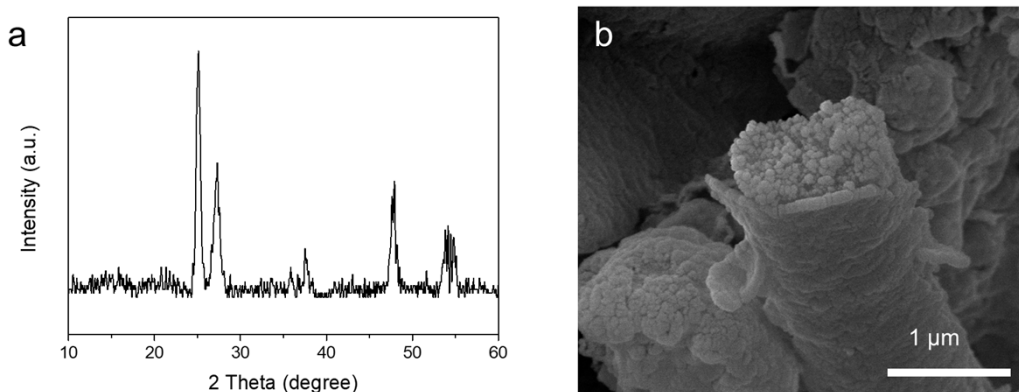
Fig. S9 a) XRD pattern and b) SEM image of PTCN-90% after four times H$_2$ evolution experiments.
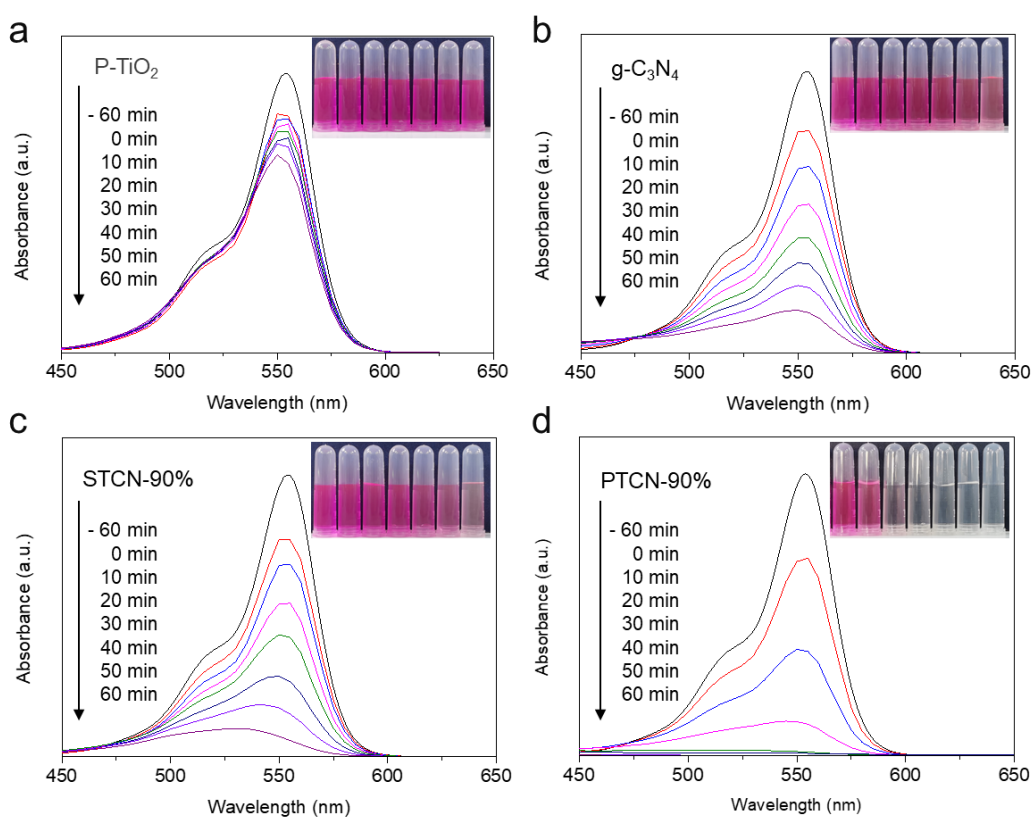
Fig. S10 The adsorption peak changes of RhB solution in a) P-TiO$_2$, b) g-C$_3$N$_4$, c) STCN-90% and d) PTCN-90% with increasing of irradiation time under visible light ($\lambda \geq 420$ nm).
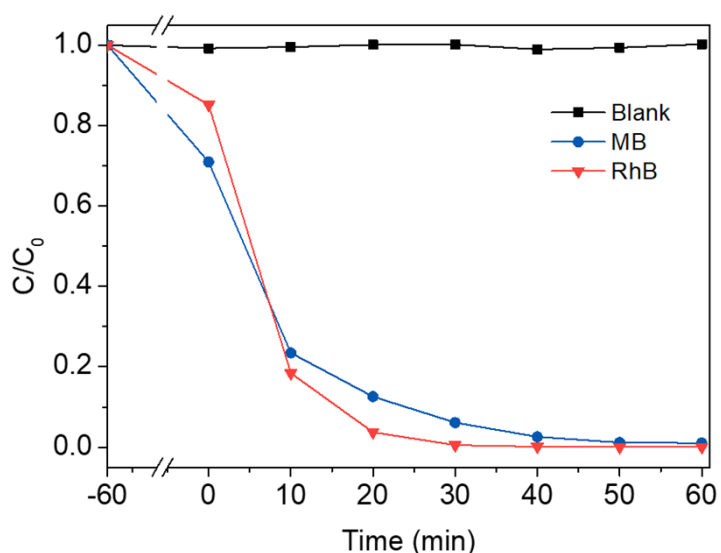
Fig. S11 Photocatalytic curves of PTCN-90% for photodegradation of RhB and MB solution in visible light.

Fig. S12 Photocatalytic phenol degradation performance of P-TiO$_2$ g-C$_3$N$_4$ and PTCN with different g-C$_3$N$_4$ content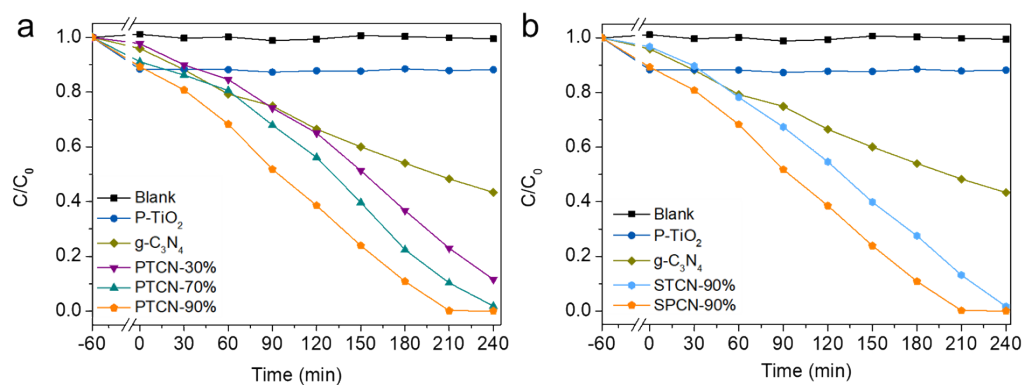 (PTCN-30%, PTCN-70% and PTCN-90%) in visible light irradiation. b) Phenol photocatalytic degradation performance for P-TiO$_2$, g-C$_3$N$_4$, PTCN-90% and STCN-90% in visible light irradiation.

After stirring in dark for 60 min to build adsorption-desorption equilibrium, the concentration of phenol almost unchanged with the exist of bare P-TiO$_2$, indicating that phenol could not act as photoactivator with TiO$_2$. PTCN-90% still exhibits the highest photodegradation performance for phenol when compared with PTCN-30% and PTCN-70%. The phenol solution was completely

degraded by PTCN-90% in 3.5 h. When compared with STCN-90%, PTCN-90% also shows better photodegradation activity, due to the core/shell structure and strong heterojunction between TiO_2 and $g-C_3N_4$.

The band structures of TiO_2 and $g-C_3N_4$ in the nanocomposite are calculated by the DRS results and the following formulas:

$$E_{CB} = \chi - E^C - 0.5E_g \#()_1.$$

$$E_{VB} = E_{CB} + E_g \#()_2.$$

where E_{CB} and E_{VB} stand for the conduction and valence band potential. χ represents the electronegativity obtained by the geometrical mean of every element. The χ values for TiO_2 and $g-C_3N_4$ are 5.81 and 4.72 eV, respectively. E^C is the free electron energy on the hydrogen scale, which is 4.5 eV. Therefore, E_{CB} and E_{VB} values of TiO_2 are calculated to be -0.23 eV and 2.85 eV, respectively. Correspondingly, E_{CB} and E_{VB} values of $g-C_3N_4$ are -1.08 eV and 1.52 eV, respectively.

Tab. S1 S_{BET} and pore volume of samples

Samples	BET Surface Area ($cm^2 \cdot g^{-1}$)	Pore Volume ($cm^2 \cdot g^{-1}$)
$S-TiO_2$	36.25	0.10
$P-TiO_2$	53.71	0.21
PTCN-90%	22.85	0.10
$g-C_3N_4$	13.20	0.05

Tab. S2 Visible light performance of TiO_2/g-C_3N_4 photocatalyst with different structures

Photocatalyst	Size	Cocatalyst	Light Condition	H_2 Production ($\mu mol \cdot g^{-1} \cdot h^{-1}$)	Ref.
TiO_2/g-C_3N_4 nanowire	150 nm	1 wt% Pt	300W Xe lamp (λ>420 nm)	63.7	[1]
TiO_2/g-C_3N_4 nanosphere	150 nm	1 wt% Pt	300W Xe lamp (λ>400 nm)	64.0	[2]
TiO_2/g-C_3N_4 nanoparticle	250 nm	1 wt% Pt	300W Xe lamp (λ>420 nm)	80.4	[3]
TiO_2/g-C_3N_4 nanoparticle	18 nm	0.5 wt% Pt	300W Xe lamp (λ>420 nm)	219.9	[4]
TiO_2/g-C_3N_4 nanosheet	-	unknown	350W Xe lamp (λ>420 nm)	210.0	[5]
TiO_2/g-C_3N_4 microsphere	10 μm	0.5 wt% Pt	300W Xe lamp (λ>420 nm)	250.0	[6]
TiO_2/g-C_3N_4 hollow nanosphere	250 nm	unknown	300W Xe lamp (AM 1.5)	195.0	[7]
TiO_2/g-C_3N_4 hollow nanosphere	100 nm	unknown	350W Xe lamp (λ>420 nm)	296.4	[8]
TiO_2/g-C_3N_4 nanofiber	330 nm	1 wt% Pt	300W Xe lamp (400~780 nm)	251.7	[9]
C@TiO_{2-x}/g-C_3N_4 nanosheet	-	3 wt% Pt	350W Xe lamp (λ>420 nm)	417.2	[10]
TiO_2/g-C_3N_4 porous nanofiber	1.41 μm	1 wt% Pt	300W Xe lamp (λ>420 nm)	436.3	our work

In comparation with other TiO_2/C_3N_4 photocatalyst, PTCN-90% exhibits high performance, with about 6.8 times higher than the nanowire and nanosphere structure,[1,2] 5.5 times the nanoparticle structure,[3] and 3.2 times the nanosheet structure.[5] When compared with STCN-90% (prepared in the same method by ourselves), PTCN-90% improves H_2 evolution performance by 40.6%.

References

1. H. Chen, Y. Xie, X. Sun, M. Lv, F. Wu, L. Zhang, L. Li and X. Xu, *Dalton Trans.*, 2015, **44**, 13030-13039.

2. X. Wei, C. Shao, X. Li, N. Lu, K. Wang, Z. Zhang and Y. Liu, *Nanoscale*, 2016, **8**, 11034-11043.

3. C. Li, Z. Lou, Y. Yang, Y. Wang, Y. Lu, Z. Ye and L. Zhu, *Langmuir*, 2019, **35**, 779-786.

4. B. Zhang, X. Peng and Z. Wang, *Nanomaterials*, 2020, **10**.

5. Y. Li, X. Feng, Z. Lu, H. Yin, F. Liu and Q. Xiang, *J. Colloid Interface Sci.*, 2018, **513**, 866-876.

6. J. Ma, X. Tan, T. Yu and X. Li, *Int. J. Hydrogen. Energ*, 2016, **41**, 3877-3887.

7. N. Guo, Y. Zeng, H. Li, X. Xu, H. Yu and X. Han, *J. Hazard. Mater.*, 2018, **353**, 80-88.

8. X. W. Shi, M. Fujitsuka, Z. Z. Lou, P. Zhang and T. Majima, *J. Mater. Chem. A*, 2017, **5**, 9671-9681.

9. X. Zhou, C. Shao, X. Li, X. Wang, X. Guo and Y. Liu, *J. Hazard. Mater.*, 2018, **344**, 113-122.

10. C. Liu, P. Wu, J. Wu, J. Hou, H. Bai and Z. Liu, *Chem. Eng. J.*, 2019, **359**, 58-68.